ARTICLE

Surface Modifications Using a Water-Stable Silanetriol in Neutral Aqueous Media

Stefan Spirk,*,† Heike M. Ehmann,† Rupert Kargl,† Natascha Hurkes,† Martin Reischl,† Jiri Novak,‡ Roland Resel,‡ Ming Wu,§ Rudolf Pietschnig,*,† and Volker Ribitsch†

Institut für Chemie, Karl-Franzens-Universität Graz, Heinrichstrasse 28/IV, 8010 Graz, Austria, Department of Chemical Technology of Materials, Graz University of Technology, Stremayrgasse 9, 8010 Graz, Austria, and Institute of Solid State Physics, Graz University of Technology, Petersgasse 16, 8010 Graz, Austria

ABSTRACT Surface modifications of glass slides employing the sterically hindered *tert*-butyl substituted silanetriol are described. To the best of our knowledge, this is the first time that a stable silanetriol has been directly used for this purpose. So far unprecedented, this process runs under neutral aqueous conditions and in the absence of organic solvents, which makes coating protocols accessible to acid-sensitive substrates. The layer thickness and surface topography are investigated by the Sarfus technique, by X-ray reflectivity, and by atomic force microscopy (AFM). These techniques yield values of 0.8 ± 0.1 (XRR) and 0.6 ± 0.2 nm (Sarfus) for layer thickness and 0.33 nm for root mean square roughness (AFM). The modified surfaces have hydrophobic and oleophilic character and contact angles (CA) between 60° (formamide, CH_2I_2) and 90° (water) are obtained. The thin coatings allow a structuring by UV/ozone treatment in order to get hydrophilic and hydrophobic compartments on the surfaces. For all coatings, surface free energies are calculated using different models. To determine the isoelectric points (IEP) of the modified surfaces, we performed zeta-potential measurements. Correlations between zeta potentials and hydrophilicity of the surfaces are shown.

KEYWORDS: silanetriol • surface modification • contact angle • zeta potential • X-ray reflectivity

INTRODUCTION

Although silanetriols, $RSi(OH)_3$, are important intermediates for the production of crosslinked silicones, only a limited number of reports on the isolation and structural characterization of this fascinating class of compounds has been made (1−17). The reason for this may originate from their high tendency to undergo condensation reactions to form stable siloxane bonds in the absence of steric protection (18, 19). If the $Si(OH)_3$ moiety is, however, sterically protected by bulky substituents, stable and chemically robust compounds can be easily obtained. The resulting stable silanetriols may themselves act as valuable starting materials for a controlled oligomerization as was shown recently (16, 20−23).

In material sciences, one of the most important techniques is the sol−gel process, which is usually performed under harsh conditions in either acidic or basic reaction media (24, 25). In the course of this procedure, silanetriols are generated by hydrolysis of trialkoxysilanes, which in subsequent reaction steps undergo condensation reactions with either a polar surface or other silanol functionalities (26, 27).

Our new approach employs the easy accessible *tert*-butyl substituted silanetriol **1** (Figure 1) for the surface modification of glass. Compound **1** is air and moisture stable and also highly soluble in water (4).

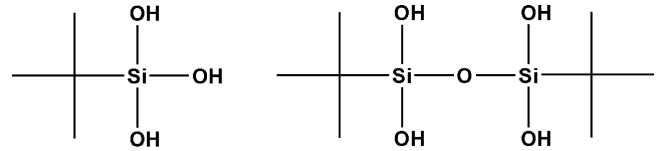

1 **2**

FIGURE 1. Silanetriol 1 and its primary condensation product, 2.

We would like to show that in neutral aqueous media it is also possible to obtain coatings that are comparable to those obtained by standard sol−gel procedures. The advantage of this method is to avoid acidic catalysts, which makes such coatings viable to be applied to acid sensitive biopolymers (e.g., polysaccharides) for the synthesis of related hybrid materials. In addition, the use of neutral conditions reduces the risk of uncontrolled condensation reactions that ultimately lead to less ordered surface structures. Moreover, the solubility of **1** in water does not require the use of organic solvents, making such a coating procedure a "green" process.

EXPERIMENTAL SECTION

All manipulations and procedures have been performed in ambient atmosphere at 298 K if not otherwise mentioned. **1** is prepared according to a published literature procedure (4). Diiodomethane (99%) and formamide (99%) were purchased from Sigma-Aldrich and used without further purification. Deuterated solvents (D_2O, d_6-DMSO) for NMR measurements were obtained from Euriso-top.

Glass substrates (slides) are cleaned by treatment with Caro's acid, freshly prepared by carefully adding H_2O_2 (33%) to H_2SO_4 (conc.) in a ratio 3:7. After 30 min the slides are rinsed three

* To whom correspondence should be addressed. E-mail: stefan.spirk@uni-graz.at (S.S.); rudolf.pietschnig@uni-graz.at (R.P.).
Received for review July 22, 2010 and accepted September 16, 2010
† Karl-Franzens-Universität Graz.
‡ Institute of Solid State Physics, Graz University of Technology.
§ Department of Chemical Technology of Materials, Graz University of Technology.
DOI: 10.1021/am100644r

Published on Web 09/28/2010

times with bidistilled water and dried in a stream of nitrogen before performing the coating experiments. For the dip-coating experiments on glass substrates, solutions containing 0.25, 0.5, and 1.0 wt % of **1** in a) bidistilled water (NTC) and b) in an acidic water/EtOH (ratio 1:1, adjusted to pH 1.5 with 1M HCl) solution (ATC) are prepared and immediately used. After the dip-coating experiments (5 min), the substrates are dried for 24 h at 60 °C in a drying oven and after cooling they are washed with bidistilled water.

Structuring into hydrophilic and hydrophobic regions can be achieved by treating the slides with ozone/UV for a period of 10 minutes at 40 °C using a grid made from aluminium. These so created hydrophilic pads (water CA: 19°) are covered with 50 μL of trimethylsilylated cellulose (28) in toluene (1.0 wt %) and the solvent is allowed to evaporate. After drying in an oven at 50 °C for 1 h (water CA: 95°), the slides are exposed to an acidic atmosphere (created by 2 mL of an aqueous 10% HCl solution in a petridish) for a period of 5 min to yield hydrophilic cellulose pads. The water contact angles of these pads (30°) fit well to data available in literature (29).

Contact angle measurements have been performed on a Dataphysics (Filderstadt, Germany) contact angle system (OCA15+) using water, diiodomethane and formamide as solvents with a drop volume of 5 μL. Solvent properties of the three testing liquids used for the calculation of the SFE can be found in the SI. At least three different glass slides of NTC and ATC have been used for contact angle determinations of every wetting liquid. On each slide, 7−10 drops are deposited. For the determination of the equilibrium structure of the liquid−solid−vapor interface, the sessile drop method has been used. For the neat solvents, surface tensions of 72.75 (water), 50.80 (diiodomethane), and 58.20 mJ/m^2 (formamide) are used for further calculations.

Surface Free Energy Calculations. In the van Oss or LWAB approach (30, 31) the surface energy is expressed as sum of the apolar interactions, called Lifshitz−van der Waals ($\gamma_{i,LW}$, includes London dispersion, Debye induction (dipole-induced dipole), and Keesom orientation (dipole−dipole forces)) and the polar Lewis acid−base ($\gamma_{i,AB,}$ often due to hydrogen bonding) interactions according to (eq 1) (30)

$$\gamma_{i,\mathrm{tot}} = \gamma_{i,\mathrm{LW}} + \gamma_{i,\mathrm{AB}} = \gamma_{i,\mathrm{LW}} + 2\sqrt{\gamma_{i,-}\gamma_{i,+}} \qquad (1)$$

where $\gamma_{i,-}$ is the electron donor and $\gamma_{i,+}$ the electron-acceptor component of the energy of the phases i. The work of adhesion W_H then can be defined according to the Young-Dupre's equation (eq 2) (30):

$$W_{\mathrm{H}} = \gamma_{\mathrm{L}}(\cos\Theta + 1) = 2(\sqrt{\gamma_{\mathrm{L,LW}}\gamma_{\mathrm{S,LW}}} + \sqrt{\gamma_{\mathrm{L},-}\gamma_{\mathrm{S},+}} + \sqrt{\gamma_{\mathrm{L},+}\gamma_{\mathrm{S},-}}) \qquad (2)$$

For a solution of this equation and the determination of the surface tension components of a solid, we employed diiodomethane ($\gamma_L = \gamma_{L,LW}$), formamide ($\gamma_L = \gamma_{L,LW} + \gamma_{L,-}$), and water ($\gamma_L = \gamma_{L,LW} + \gamma_{L,+} + \gamma_{L,-}$).

Quartz-Crystal Microbalance. Adsorption of **1** has been monitored by a quartz-crystal microbalance with dissipation monitoring apparatus, QCM-D (model E4, QSense AB, Göteborg, Sweden) using QSX 303 sensors (SiO_2, 50 nm). Each sample has been measured at least three times at 20 °C at constant flow (0.1 mL/min, 1.0 wt % solutions of **1**) in a Q-Sense standard flow module (QFM 401). Prior to adsorption of **1** surfaces are rinsed with Milli-Q water for a period of 10 minutes at a flow rate of 0.1 mL/min. For the calculation of adsorbed mass, the Sauerbrey equation (32) has been employed (eq 3)

$$\Delta f = \frac{-C\Delta m}{n} \qquad (3)$$

where Δf is the observed frequency change, C is the Sauerbrey constant (17.7 ng Hz^{-1} cm^{-2} for a 5 MHz crystal), n is the overtone number (n = 1,3,5,7; has been considered by the software automatically) and Δm is the change in mass.

Zeta Potential Determination. Zeta potentials have been determined on an apparatus which had been constructed and built in our group (33). The determination of zeta potentials is carried out using the oscillating streaming potential method (EKA-Oszi). This method differs from other approaches because of the creation of an oscillatory flow of electrolyte solutions through or along the sample. Streaming potential and applied pressure are measured simultaneously together with the conductivity, temperature and pH value of the electrolyte solution. The wide range of applicable flow frequencies and amplitudes provides a fast and precise measurement enabling streaming potential detection at rather high ionic strength and in a very short time regime (< 1 s). This allows the monitoring of the kinetics of adsorption processes. The zeta potential (ζ) is calculated using the Smoluchowski equation (eq 4) (34), whereby ζ is the zeta potential, dU is the streaming potential, dp the pressure loss, η the viscosity, κ the conductivity of the electrolyte solution, ε_0 and ε are the permittivity of free space and the dielectric constant of the electrolyte solution, respectively.

$$\zeta = \frac{du}{dp}\frac{\eta}{\varepsilon_r\varepsilon_0}\kappa \qquad (4)$$

The pH range used for the measurements was 2.4−9.8. As electrolyte, an aqueous KCl (1 mM) solution was used.

X-ray Reflectivity. XRR measurements have been performed using a Bruker AXS D8 Discover X-ray diffractometer equipped with a collimating and monochromating graded parabolic multilayer mirror on the primary-beam side and two collimating slits at the secondary side. CuKα radiation of wavelength λ = 1.542 Å was employed. Experimental data simulations and fits were performed using a freeware software GenX (35). Here, XRR simulations are calculated using the Parrat recursive formula (36). A Gaussian type roughness of surfaces and interfaces is assumed and it is taken into account by applying corrective factors for interface reflection coefficients according to the Croce−Nevot model (37). The fitting parameters in the search for the best simulation of the XRR were the coating thickness d, the refraction index of the coating, and SiO_x surface roughness R_q.

Sarfus and AFM. Optical microscopy (Sarfus) is done on a polarization light microscope from Leica (Wetzlar, Germany). Surfs were obtained from Nano Lane (Montfort-le-Gesnois, France) and analyzed using the Sarfusoft program. A more detailed description of this method can be found elsewhere (38). For layer thickness determination, 15 surfs were used (only half of each surf was covered with the coating solution during dipping and the height difference between the uncoated and coated part was calculated).

Atomic force microscopy images are recorded on a Nanoscope V Multimode AFM (Veeco) using silicon cantilevers TESP7 from Veeco Instruments with an average spring constant of 40 N/m, tip radius of 8 nm and resonance frequency of 320 kHz. Image processing, analysis, and root mean square roughness calculation are performed with WSxA freeware (39).

NMR Spectroscopy. ^{29}Si-NMR spectra have been performed on a Bruker Avance III at a larmor frequency of 59.6273 MHz for ^{29}Si using TMS as a reference at 298 K. All spectra have been

Table 1. Comparison of the Contact Angles (deg (±sd)) on Glass Slides Using 1 via ATC and NTC Using Different Wetting Liquids on Glass Slides

	0.25 wt % ATC	0.25 wt % NTC	0.5 wt % ATC	0.5 wt % NTC	1.0 wt % ATC	1.0 wt % NTC	Piranha glass
H_2O	77 (±1)	86 (±3)	74 (±2)	89 (±2)	74 (±1)	92 (±1)	14 (±2)
$HCONH_2$	66 (±2)	65 (±2)	60 (±1)	68 (±2)	60 (±1)	68 (±2)	10 (±3)
CH_2I_2	60 (±1)	59 (±3)	61 (±3)	64 (±2)	62 (±2)	62 (±1)	50 (±2)

Table 2. Surface Free Energies of the Modified Surfaces Calculated Using the van Oss Model[a]

	0.25 ATC	0.25 NTC	0.5 ATC	0.5 NTC	1.0 ATC	1.0 NTC	untreated
γ_{total}	30.9	32.3	33.8	28.8	33.6	29.7	57.4
γ_{LW}	28.7	29.1	27.8	25.6	27.7	27.5	34.2
γ_+	0.1	0.6	0.8	0.9	0.7	0.6	2.6
γ_-	12.8	4.3	11.4	2.9	12.7	2.0	51.1

[a] Concentrations are given in wt %. All SFE are given in mJ/m^2. Estimated errors <5%.

measured using an inverse-gated pulse sequence with pulse angles of 30° and D1 of 20 s.

RESULTS AND DISCUSSION

We investigate two cases in our study. The first involves a dip-coating procedure by a sol–gel route in acidic medium which is a standard method in our laboratories. In the following, these samples are referred to as ATC (acid-treated coatings). In the second case, neutral aqueous conditions are used for surface modification (NTC, neutral-treated coatings).

Contact Angle Determinations and Surface Free Energy (SFE) Calculation. We found major differences in the absolute values for the CAs between silanetriol coatings derived from ATC and NTC for all used test liquids (water, formamide, CH_2I_2).

For ATC, water contact angles between 74 and 77° have been determined. CAs seem to be slightly dependent on the concentration, however, the differences are small and not significant (Table 1). In addition, contact angles are not changing when extending the dip coating times from five to 30 minutes. In contrast, NTC show higher contact angles and they are increasing with increasing concentration of the stock solutions used for coating. The highest CA could be obtained for the most concentrated solution (1.0 wt %) exhibiting a value of 92° after 5 minutes of dip-coating. However, when the dip-coating time is extended to 30 min for the 0.25 and 0.5 wt % solutions of **1**, similar values (91 ± 2°) are observed.

The determination of the contact angles of different test liquids of defined polar and dispersive attributes allows the calculation of the surface free energies (SFE) using different theoretical models. All investigated models (Equation-of-state, OWRK model (40–42), Wu-theory (43)) show the same trends (for details, see the Supporting Information), therefore in the following we will discuss only the results derived from the van Oss model (30, 31) enabling the determination of Lewis-donor and Lewis-acceptor properties of the surface. For this purpose, contact angles of three liquids, namely water, formamide, and diiodomethane, are used for SFE determinations (Table 2).

In comparison to unmodified glass slides, SFE of the ATC and NTC are significantly lower with differences of 24 to 30 mJ/m^2. When looking at the nature of contributions, the dispersive (γ_{LW}) and the acidic (γ_+) parts of the SFE remain nearly unaffected by the coating ($\Delta\gamma_{LW} = 7-9$ mJ/m^2, $\Delta\gamma_+ = 2$ mJ/m^2) while the basic contributions, γ_-, show a strong decrease ($\Delta\gamma_- = 39-49$ mJ/m^2) compared to glass. The main difference between ATC (11–12 mJ/m^2) and NTC (2–4 mJ/m^2) samples can be found in the contributions derived from γ_-. In the case of NTC, surface adsorption of hydrated OH^- groups (Lewis/Bronsted base) is preferred, caused by their larger adsorption enthalpy in comparison to hydrated H^+ ions.

The differences between ATC and NTC in terms of CA and SFE may be explained by the mechanisms how the silane binds to the surface during the dipping procedure. It is known that condensation rates of silanols are much higher in strongly acidic/basic solutions than in neutral media (44); therefore, intermolecular condensation with other silanetriol molecules and/or with silanol functionalities on the surface should be favored for ATC. In contrast, at neutral pH, condensation rates for silanols are significantly lower; therefore adsorption processes on surface silanol functionalities should be dominant for NTC, whereas condensation should be negligible. Several possible adsorption and bonding modes are depicted in Scheme 1. These assumptions are also corroborated by ^{29}Si-NMR spectroscopy which is a very sensitive probe to monitor condensation reactions of silanols. For ATC solutions, even after a short period of time (20 minutes), significant amounts (~15%) of the primary condensation product, the tetrahydroxydisiloxane, **2** (Figure 1), can be detected (δ ^{29}Si: −50.4 in EtOH with a capillary filled with d_6-DMSO). In contrast, the ^{29}Si-NMR spectrum (D_2O) of the NTC solutions exclusively shows a peak at −38.7 ppm corresponding to **1**. Even after several hours, no signs of condensation can be observed in the ^{29}Si-NMR spectra.

In the case of NTC, we suggest that condensation of **1** with surface OH groups occurs upon drying. Without drying the NTC samples in an oven overnight (60 °C), **1** is not irreversibly bound to the surface and can be easily removed by washing with water resulting in low water CA. In contrast, ATC showed higher contact angles (60–65°, data not shown) without drying, indicating at least partly covalent binding on the surface at this stage of the coating procedure.

A possibility to verify these assumptions are adsorption studies using a quartz-crystal microbalance with dissipation (QCM-D) (45). This technique allows an in situ monitoring of adsorption processes on the solid–solution interface with high precision and accuracy over a wide mass range.

In a first step, adsorption of neutral aqueous solutions (1 wt %) of **1** on SiO_2 coated quartz crystals was investigated. According to the Sauerbrey equation (32), adsorption of 139

Scheme 1. Postulated Surface Interactions and Reactions of 1 with Glass Surfaces (dotted lines indicate hydrogen bridges)

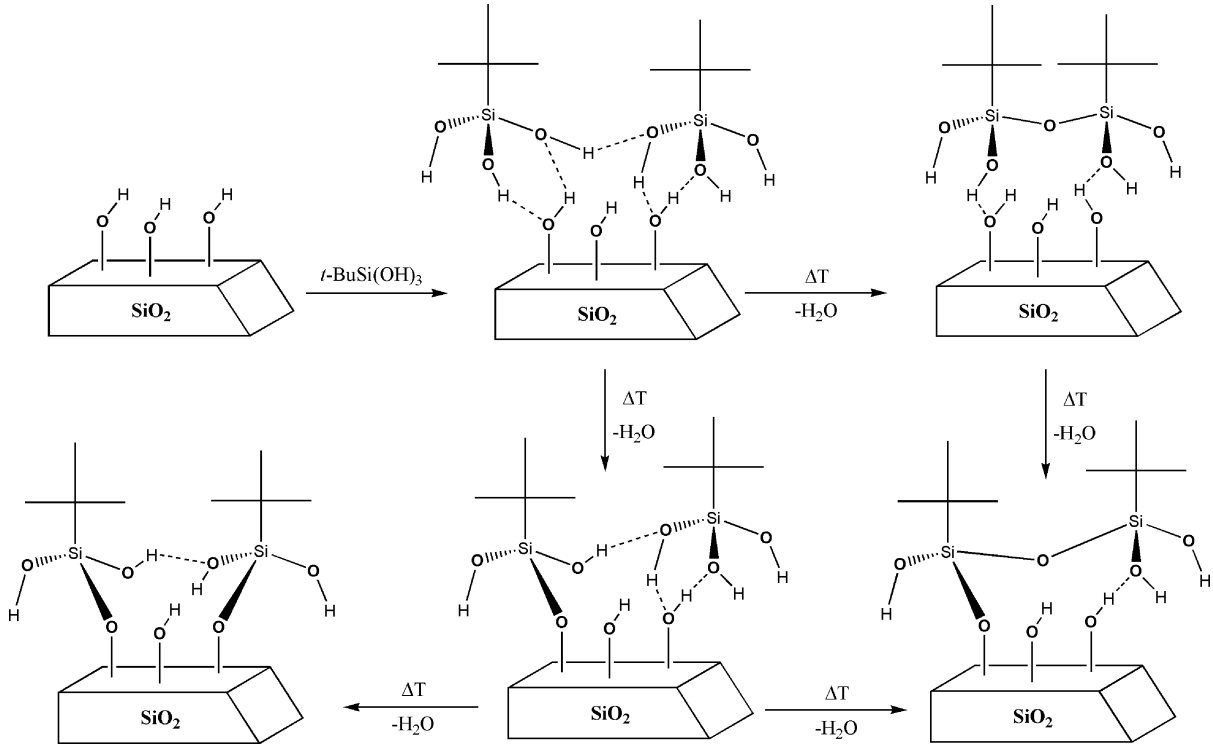

± 9 ng/cm^2 of **1** was found; however, upon washing with water the silanetriol desorbed quantitatively from the surface (46). In contrast, by using an acidic 1.0 wt % solution (H_2O/EtOH 1:1, pH 1.5) irreversible adsorption of up to 860 ng/cm^2 of the silane onto the surface was observed; it can be concluded that in case of ATC condensation of the surface Si−OH groups with the silanetriol/tetrahydroxydisiloxane takes place even without the drying step. The water contact angles on the quartz-crystals after rinsing with water showed similar results as described above (NTC: 20°, ATC: 59°).

Nevertheless, results derived from adsorption of neutral solutions are highly reproducible with narrow error margins, whereas those obtained for the acidic solutions vary in a wide range between 160 and 860 ng/cm^2. Although we cannot explain the reason for this behavior at the moment, it is obvious that in acidic solutions, the silane irreversibly binds to the surface. The detailed investigation of these adsorption/bonding processes in acidic solution is currently in progress and a discussion at this point would be premature.

Surface Morphology, Layer Thickness, Structuring, and Zeta-Potential Determinations. To get additional insights into the thickness of the coatings (1 wt %, NTC), we employed X-ray specular reflectivity (XRR) and the Sarfus technique. However, for these methods, glass slides cannot be used and therefore our coating procedure was performed on silicon wafers coated with 100 nm SiO_x (XRR, AFM) and surfs (Sarfus) assuming that this will not have a significant effect on coating thickness and roughness. Layer thicknesses obtained by both methods are very similar and range between 0.8 ± 0.1 nm (XRR) and 0.6 ± 0.2 nm (Sarfus) for coatings derived from 1 wt % solutions. Measured XRR data were fitted with reflectivity simulations based on calculations corresponding to a model silanetriol layer on top of the SiO_x layer and Si substrate.

The measured data for XRR together with the data best fit are shown in Figure 3. The coating thickness can be already estimated from the position of the maximum of the enhanced intensity at $Q_z = 0.52$ nm^{-1} (indicated by a vertical line in Figure 3), arising from positive interference of X-rays reflected at the air/coating and coating/substrate interfaces. The position of the first thickness oscillation maxima is in the first approximation related to the thickness of the film according to eq 5

$$Q_z^{\max} = \frac{2\pi}{d} = \frac{4\pi \sin(2\theta_{\max}/2)}{\lambda} \qquad (5)$$

where λ is the wavelength of X-rays and $2\theta_{\max}$ is a scattering angle, at which the maximum appears (47). From here, we obtain a rough estimate of the film thickness $d = 1.2$ nm. However, the refraction of X-rays at the air/coating interface and thickness oscillation maxima of higher order have to be taken into account to get a better estimation (47). At the same time, the refraction index of the coating is a priori unknown and we observe only the first-order thickness oscillation, whereas the higher order oscillations intensity is hidden below the scattering background. Instead, fitting of the experimental data using model XRR curves was performed.

A good agreement between the experimental data and the best fit (see the red and green curve, respectively, in

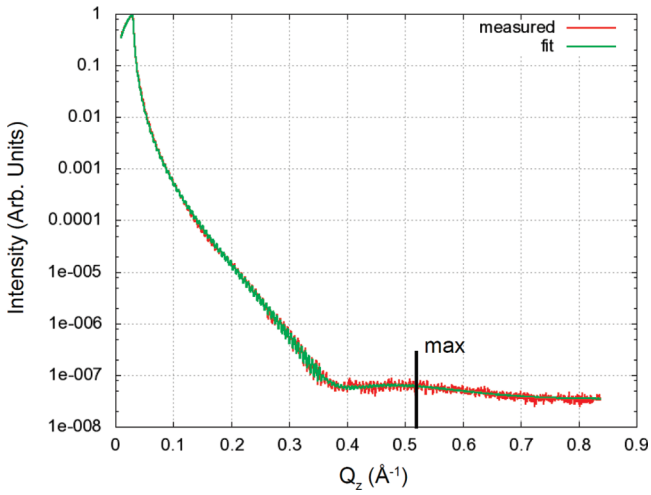

FIGURE 2. Measured specular X-ray reflectivity for a neutral treated coating prepared at concentration 1 wt % (red curve) and the best fit of the measured data (green) obtained. The vertical line indicates the position of a maximum arising from an interference of X-rays reflected at the coating/layer and coating/substrate interfaces.

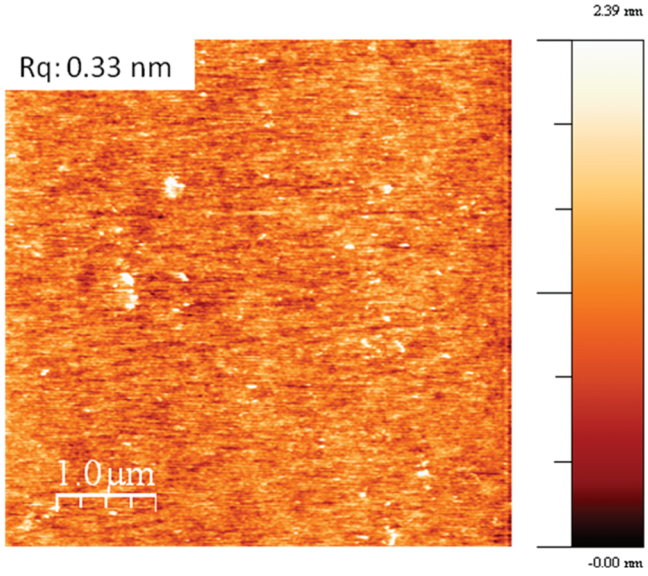

FIGURE 3. 5 × 5 μm^2 AFM image of a silicon wafer (100 nm SiO_x on top of the surface) coated with 1.0 wt % *tert*-butylsilanetriol in water, *z*-scale 2.4 nm. The bright spots represent islands of aggregated material of 1. Possibly, these islands consist of adsorbed material that was not removed by the washing step.

Figure 2) was obtained for an above stated coating thickness of 0.8 ± 0.1 nm, electron density of ρ_{el} = (380 ± 40) nm^{-3}, the coating surface root mean square roughness (R_q) of 0.35 ± 0.05 nm, and R_q of the SiO_x substrate of 0.23 ± 0.03 nm.

Indeed, the surface roughness of the silanetriol coating partially originates from the roughness of the underlying substrate. Similar R_q values of the coatings (0.33 nm) have been found by AFM (Figure 3).

For layer thickness determination by Sarfus, coatings were deposited only on one half of each surf. Layer thickness was measured with respect to the reference of the uncoated part.

On the basis of the agreement between the layer thickness determined from XRR and Sarfus and the length of the molecule chain 0.5 to 0.6 nm, obtained from previous single-crystal X-ray studies (17) on **1**, we argue that a monolayer of standing molecules of **1** was formed during the neutral coating process. In addition, the high water contact angles of NTC (corresponding to hydrophobic alkyl chains at the interface) corroborate this description of the synthesized coatings.

For additional information on surface properties, samples have been subjected to zeta-potential measurements. Although the interpretation of zeta potentials in case of polymer surfaces is sometimes tricky because of swelling of the polymer chains, for our surfaces it can be directly used to assess the amount of free OH groups on the surface qualitatively. For nonswelling surfaces with a large amount of OH groups, zeta potentials should exhibit lower potentials than those with a low OH content. Therefore, such lower potentials should also correlate to water contact angles and surface free energies.

In all determinations, the potential has been measured as a function of the pH value (Figure 4). All investigated samples show reduced negative potential in comparison to glass which is closely related to the smaller amount of free OH groups available at the surface. At pH 10, the charge differences between pure glass and ATC are in the range of 40−50 mV. ATC with the lowest concentration (0.25 wt %) show a significant lower zeta potential at pH 10 (−73 mV) in comparison to the other samples (ca. −57 mV, see the Supporting Information).

In contrast, in case of NTC almost no concentration dependence is observed. The plateau value at pH 10 is reduced from −90 mV (uncoated glass) to −35 to −39 mV. Regarding the curve shape, the linearization behavior is even more pronounced compared to ATC, which is characteristic for less-polar, hydrophobic surface properties.

In both cases, a correlation between water contact angles and surface free energy data with the zeta potentials can be found; small water contact angles lead to low zeta potentials. Also increasing contributions to surface free energy derived from γ- (compare: 11.4−12.8 mJ/m^2 for ATC vs. 2.0−4.2 mJ/m^2 for NTC) can be directly correlated to higher zeta potentials.

Finally, the investigated surfaces exhibit lower IEP (3.5−3.8) than freshly cleaned glass substrates (IEP = 4.2).

The layer thickness in the nanometer range inspired us to consider also structuring of the hydrophobic surfaces. It is known that ozone in combination with UV light is capable of oxidizing different kinds of surfaces. Upon treatment of our modified glass substrates with UV/ozone using a grid, hydrophilic compartments on a hydrophobic surface are obtained. For sensor applications, however, cellulose derivatives used in biotechnology are even more interesting, e.g., nitrocellulose in Northern, Western, and Southern blots. In fact, the controlled deposition of cellulose is difficult because of the poor solubility of cellulose in common organic solvents. Therefore, we decided to take a different approach that uses a soluble cellulose derivative that is converted back to cellulose after deposition. Trimethylsilylated cellulose appeared to us the most promising candidate for this

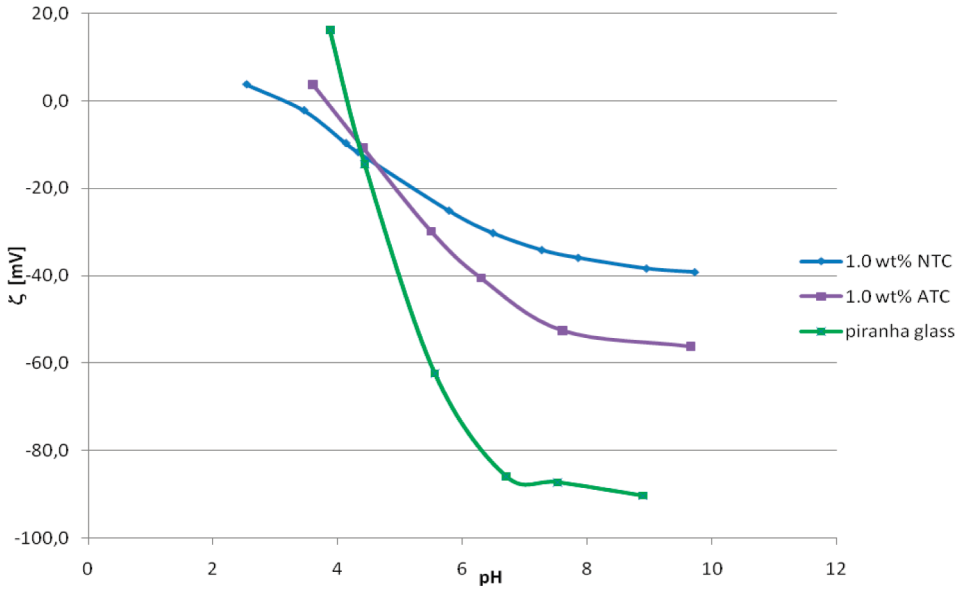

FIGURE 4. Comparison of the zeta potentials of ATC and NTC to glass as a function of pH value.

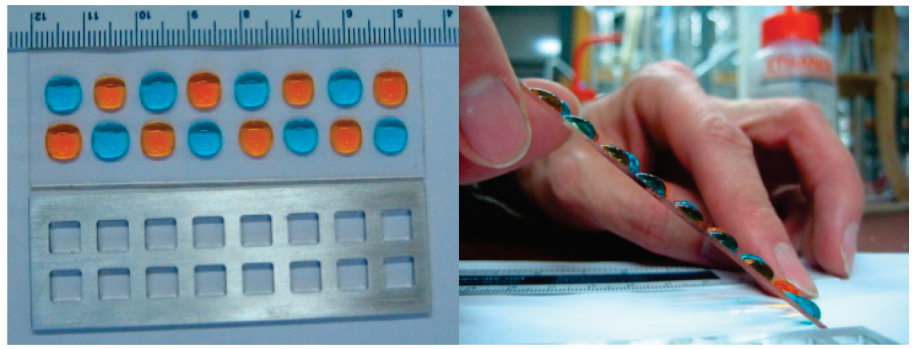

FIGURE 5. Photograph of a hydrophobized glass slide with hydrophilic cellulose pads. On the pads, colored water drops are deposited that do not migrate into the hydrophobic regions of the glass slide.

purpose. In a second step, the silylated cellulose could indeed be transformed easily to cellulose via standard desilylation reactions while retaining the hydrophobic grid pattern (48). Preliminary tests demonstrate that the resulting hydrophilic compartments confined by a hydrophobic grid structure are suitable to serve as array slides for water-based assays. A photograph of the patterned surfaces is depicted in Figure 5.

SUMMARY AND CONCLUSION

We showed for the first time that surface modifications of glass substrates using silanetriols can be performed in neutral aqueous solutions avoiding the use of organic solvent. The results in terms of contact angles, surface free energies, and stability are comparable to those obtained via classical sol−gel-derived processes. In addition, the use of neutral conditions causes significant enhancements of the surface hydrophobicity and CAs of up to 92° can be obtained. Layer thickness is between 0.6 and 0.8 nm, which is a strong indication for the deposition of monolayers on the surface. Although we investigated only surface modifications of glass substrates, it is obvious that similar results can be obtained for surfaces possessing free OH groups such as alumina or titania. A controlled patterning of hydrophobic coatings was also demonstrated to generate cellulose pads on a hydrophobic surface.

Our procedure is also advantageous with respect to the surface modification of biopolymers such as polysaccharide films, which easily degrade when in prolonged contact with acids. A future goal is, however, to synthesize hybrid materials using such neutral aqueous solutions; investigations of the general applicability of this method towards polysaccharides are underway.

Acknowledgment. This work was financially supported by the 7th framework program of the European Union (Surfuncell), the Austrian Science Funds FWF (P17882−N11, P20575−N19, S9708), and the fFORTE Wissenschafterinnenkolleg FreChe Materie. Dr. Stefan Köstler is gratefully acknowledged for fruitful discussions.

Supporting Information Available: Additional zeta-potential data, solvent properties used for surface free energy determination, as well as surface free energy data for the WU, OWRK, and van-Oss models, QCM/adsorption of NTC (PDF). This material is available free of charge via the Internet at http://pubs.acs.org.

REFERENCES AND NOTES

(1) Takiguchi, T. *J. Am. Chem. Soc.* **1959**, *81*, 2359.
(2) Buttrus, N. H.; Damja, R. I.; Eaborn, C.; Hitchcock, P. B.; Lickiss, P. D. *J. Chem. Soc., Chem. Commun.* **1985**, 1385.
(3) Al-Juaid, S. S.; Buttrus, N. H.; Damja, R. I.; Derouiche, Y.; Eaborn, C.; Hitchcock, P. B.; Lickiss, P. D. *J. Organomet. Chem.* **1989**, *371*, 287.
(4) Winkhofer, N.; Roesky, H. W.; Noltemeyer, M.; Robinson, W. T. *Angew. Chem.* **1992**, *104*, 670.
(5) Murugavel, R.; Chandrasekhar, V.; Voigt, A.; Roesky, H. W.; Schmidt, H. G.; Noltemeyer, M. *Organometallics* **1995**, *14*, 5298.
(6) Jutzi, P.; Strassburger, G.; Schneider, M.; Stammler, H.-G.; Neumann, B. *Organometallics* **1996**, *15*, 2842.
(7) Murugavel, R.; Chandrasekhar, V.; Roesky, H. W. *Acc. Chem. Res.* **1996**, *29*, 183.
(8) Jutzi, P.; Schneider, M.; Stammler, H. G.; Neumann, B. *Organometallics* **1997**, *16*, 5377.
(9) Kornev, A. N.; Chesnokova, A.; Zhezlova, E. V.; Kurskii, Y.; Alakarenko, N. P. *Russ. Chem. Bull.* **1999**, *48*, 1563.
(10) Schneider, M.; Neumann, B.; Stammler, H. G.; Jutzi, P. *Monatsh. Chem.* **1999**, *130*, 33.
(11) Cerveau, G.; Corriu, R. J. P.; Dabiens, B.; Le Bideau, J. *Angew. Chem. (Int. Ed.)* **2000**, *39*, 4533.
(12) Pietschnig, R.; Belaj, F.; Tirrée, J. J. *Organometallics* **2004**, *23*, 4897.
(13) Prabusankar, G.; Murugavel, R.; Butcher, R. J. S. *Organometallics* **2004**, *23*, 2305.
(14) Kim, J. H.; J.S., H.; Lee, M. E.; Moon, D. H.; Lah, M. S.; Yoo, B. R. *J. Organomet. Chem.* **2005**, *690*, 1372.
(15) Spirk, S.; Belaj, F.; Baumgartner, J.; Pietschnig, R. *Z. Anorg. Allg. Chem.* **2009**, *635*, 1048.
(16) Unno, M.; Tanaka, T.; Matsumoto, H. *J. Organomet. Chem.* **2003**, *686*, 175.
(17) Pietschnig, R.; Belaj, F. *Inorg. Chim. Acta* **2005**, *358*, 444.
(18) Lickiss, P. D. *Adv. Inorg. Chem.* **1995**, *42*, 147.
(19) Lickiss, P. D. In *Chemistry of Organic Silicon Compounds*; Rappoport, Z.; Apeloig, Y., Eds.; Wiley: Chichester, U.K., 2001; Vol. 3.
(20) Unno, M.; Alias, S. B.; Saito, H.; Matsumoto, H. *Organometallics* **1996**, *15*, 2413.
(21) Spirk, S.; Belaj, F.; Nieger, M.; Pietschnig, R. *Dalton. Trans.* **2009**, 163.
(22) Lickiss, P. D.; Litster, S. A.; Redhouse, A. D.; Wisener, C. J. *J. Chem. Soc., Chem. Commun.* **1991**, 173.
(23) Suzuki, J.; Shimojima, A.; Fujimoto, Y.; Kuroda, K. *Chem.—Eur. J.* **2008**, *14*, 973.
(24) Corriu, R. J. P.; Boury, B. In *Chemistry of Organic Silicon Compounds*; Rappoport, Z.; Apeloig, Y., Eds.; Wiley: Chichester, U.K., 2001; Vol. 3.
(25) Avnir, D.; Klein, L. C.; Levy, D.; Schubert, U.; Wojcik, A. B. In *Chemistry of Organic Silicon Compounds*; Rappoport, Z.; Apeloig, Y., Eds.; Wiley: Chichester, U.K., 2001; Vol. 2.
(26) Solomun, T.; Mix, R.; Sturm, H. *ACS Appl. Mater. Interfaces* **2010**, *2*, 2171.
(27) Yang, S.; Kwak, S.-Y.; Jin, J.; Bae, B.-S. *ACS Appl. Mater. Interfaces* **2009**, *1*, 1585.
(28) Koehler, S.; Liebert, T.; Heinze, T. *J. Polym. Sci., Polym. Chem.* **2008**, *46*, 4070.
(29) Kontturi, E.; Thüne, P. C.; Niemantsverdriet, J. W. *Langmuir* **2003**, *19*, 5735.
(30) van Oss, C. J.; Chaudhury, M. K.; Good, R. J. *Chem. Rev.* **1988**, *88*, 927.
(31) van Oss, C. J. *Interfacial Forces in Aqueous Media*; Dekker: New York, 1994.
(32) Sauerbrey, G. *Z. Phys.* **1959**, *155*, 206.
(33) Reischl, M.; Köstler, S.; Kellner, G.; Stana-Kleinschek, K.; Ribitsch, V. *Rev. Sci. Instrum.* **2008**, *79*, 113902.
(34) Smoluchowski, M. *Handbuch der Elektrizität und des Magnetismus*; Barth-Verlag: Leipzig, Germany, 1921.
(35) Björck, M.; Andersson, G. *J. Appl. Cryst.* **2007**, *40*, 1174.
(36) Parratt, L. G. *Phys. Rev.* **1954**, *95*, 359.
(37) Névot, L.; Croce, P. *Rev. Phys. Appl.* **1980**, *15*, 761.
(38) Ausserre, D.; Valignat, M.-P. *Nano Lett.* **2006**, *6*, 1384.
(39) Horcas, I.; Fernandez, R.; Gomez-Rodriguez, J. M.; Colchero, J.; Gomez-Herrero, J.; Baro, A. M. *Rev. Sci. Instrum.* **2007**, *78*, 013705.
(40) Owens, D. K.; Wendt, R. C. *J. Appl. Polym. Sci.* **1969**, *13*, 1741.
(41) Kaelble, D. H.; Uy, K. C. *J. Adhes.* **1970**, *2*, 50.
(42) Rabel, W. *Farbe Lack* **1971**, *77*, 997.
(43) Wu, S. *Polymer Interface and Adhesion*; Marcel Dekker: New York, 1982.
(44) Brook, M. A. *Silicon in Organic, Organometallic, and Polymer Chemistry*; Wiley: New York, 2000.
(45) Marx, K. A. *Biomacromolecules* **2003**, *4*, 1099.
(46) The theoretical mass of a monolayer consisting of silanetriol **1** was calculated to be 251 ng/cm^2 on the basis of the structure obtained in single-crystal X-Ray diffraction.
(47) Pietsch, U.; Holý, V.; Baumbach, T. *High-Resolution X-ray Scattering*; Springer-Verlag: New York, 2004.
(48) Schaub, M.; Gerhard, W.; Wegner, G.; Stein, A.; Klemm, D. *Adv. Mater.* **1993**, *5*, 919.

AM100644R